

Integration of Arc-jet in Impulse Facility for Hypervelocity Aerothermal Testing with Ablation

Eric Won Keun Chang^{*}, Chinmay Joglekar[†], Matthew McGilvray[‡], and Tobias A. Hermann[§]
University of Oxford, Osney Mead, Oxford OX2 0ES, United Kingdom

Arc-jets and impulse facilities have been extensively used to investigate the flow physics of planetary re-entry, but they each address different aspects of re-entry flow-fields. This work presents a conceptual design of a dual-facility setup, utilising an arc-jet as a model preheating device in the impulse test facility. This novel preheating apparatus will replicate realistic ablation coupling effects in hypervelocity flows. This paper outlines the major challenges and key considerations for the system integration of arc-jet in the T6 Stalker Tunnel. A small-scale arc-jet facility, OPG1, is currently being developed at the University of Oxford to test the plasma generator, model movement system, and sub-components for the expansion tube testing. Analyses were performed to examine the thermal and structural loads on the model movement system exposed to both plasma and hypervelocity flow. The results showcased that the model movement system will effectively serve dual-facility operations.

I. Nomenclature

H	=	enthalpy
M	=	Mach number
\dot{m}	=	mass flow rate
p	=	pressure
R	=	nose radius
T	=	temperature
ρ	=	density
U	=	flight-equivalent velocity
v	=	velocity
<i>subscripts</i>	=	
1	=	shock tube
5	=	acceleration tube
$s1$	=	primary shock
$s2$	=	secondary shock
<i>cone</i>	=	15° conehead probe
$t, flow$	=	total, expansion tube flow
$t, plasma$	=	total, plasma flow
w	=	wall
∞	=	freestream

II. Introduction

ATMOSPHERIC re-entry vehicles experience extreme aerothermal loads. The large kinetic energy of the high-velocity air gets transferred into internal energy through the shock layer around a spacecraft. Heat shield ablates due to the large surface heat flux and continuously decomposes during the entry. At superorbital entry velocities above 10 km/s, the portion of radiative heat flux becomes the same order of magnitude as convective heating [1] that lead to

^{*}Postdoctoral Research Assistant, Oxford Thermofluids Institute, Department of Engineering Science.

[†]Masters Student, Oxford Thermofluids Institute, Department of Engineering Science.

[‡]Professor, Oxford Thermofluids Institute, Department of Engineering Science.

[§]UKRI Future Leaders Fellow, Departmental Lecturer, Oxford Thermofluids Institute, Department of Engineering Science.

ablation-radiation coupling in the flow-field with high uncertainties [2–4]. A significant contribution of radiative heat flux comes from the vacuum ultraviolet (VUV) wavelength, owing to strong atomic emissions [5, 6]. A strong coupling between flow-field and injected ablation species is present, altering the thermodynamic parameters in the flow-field, such as chemical species concentration, enthalpy and velocity field. These complex flow phenomena pose a challenge to replicate in ground-based experiments.

Two types of experimental facilities are extensively used to simulate planetary re-entry aerothermodynamics around realistic test models [7]. First, arcjet wind tunnels [8–12] can supply high-enthalpy flows for a continuous duration, which is suitable for investigating the interaction between the flow and the heat shield material. However, the test flow lacks the aerodynamic similarity of a complete flow-field as only the post-shock stagnation streamline region is replicated [13]. Second, impulse facilities such as shock/expansion tubes [14, 15] use a rapid release of stored energy to generate high total pressure and enthalpy matched flow conditions, but their micro-to-milliseconds order test duration is insufficient to reach the equilibrium surface temperature during the steady test-time. This short test duration requires a model preheating methodology to match the wall-to-total temperature ratio (T_w / T_∞) expected in hypersonic flight. Previous preheating methods in impulse facilities relied on the electrical heating of high-resistivity materials such as graphite [16–24] to reach high wall temperatures. The advantage of this method is in its simplicity, yet it requires the use of electrically conductive materials and specific geometries to achieve effective resistive heating. More importantly, the mass blowing effect and the gas-surface interaction of an ablating heat-shield are largely neglected as the heat is introduced volumetrically into the test model rather than by a surface heat flux. Regarding this, recent developments of small-scale arcjets [25–30] motivated their use as a preheating device for the sub-scale test models before being exposed to the hypersonic flow. This dual-facility concept was originally discussed in a reference [31].

This work presents a conceptual design of integrating an arcjet in an expansion tube. The integration will enable realistic preheated model experiments in hypervelocity flows. As a first step, a small-scale arcjet system [32] is currently being developed to examine the feasibility of a plasma generator, model movement system, and sub-component systems. This paper focusses on the dual-facility preheating methodology, including the expansion tube flow conditions and necessary considerations for the implementation within the facility test section.

III. Plasma Generator System

A. Overview

Osney Plasma Generator 1 (OPG1) "Osneyblast" is a standalone 21.5kW thermal arc-jet facility being developed in the Southwell Laboratory at the University of Oxford. OPG1 is also designed as a testbed of the plasma generator and sub-component systems for the integration in the T6 Stalker Tunnel. Figure 1 illustrates a schematic of the OPG1 facility. A DC power supply provides an electric current to the welding torch located inside a 20-inch cylindrical test chamber. When the power is turned on, electrical arc is formed between the tungsten cathode of the torch and the bespoke copper nozzle, heating argon gas to a plasma state. Then, the plasma is expanded through the nozzle and reaches the test model. The model is mounted on a movement system to traverse. A plasma exhaust channel downstream of the model movement system extracts the ablated products and vaporised resins to maintain a desired pressure inside the test chamber. Various feed-throughs for evacuation, water-cooling, electricity, gas, and pressure/temperature sensors, are installed around the chamber. The system operation is recorded by a data acquisition system. More details are provided in a sister paper [32].

IV. Dual-Facility Preheating System Methodology

A. T6 Stalker Tunnel in Expansion Tube Configuration

T6 Stalker Tunnel [33, 34] is a recently commissioned free-piston driven impulse facility at the University of Oxford. The facility can operate in reflected shock tunnel, expansion tube/tunnel [35], and non-reflected shock tube [36, 37] configurations. An expansion tube configuration was selected for the present investigation to generate the highest total enthalpy and density re-entry test flows. Fig. 2 shows the schematic of the T6 expansion tube configuration. The expansion tube consists of a free-piston driver, shock tube, acceleration tube with a tertiary barrel, test section, and dump tank. The flow direction is from left to right. The experimental preparation begins with an evacuation of the entire section. Then, gases are filled in each section with shock tube pressure p_1 and acceleration tube pressure p_5 , which are separated by primary and secondary diaphragms. When the tunnel is fired, high-pressure air in the reservoir

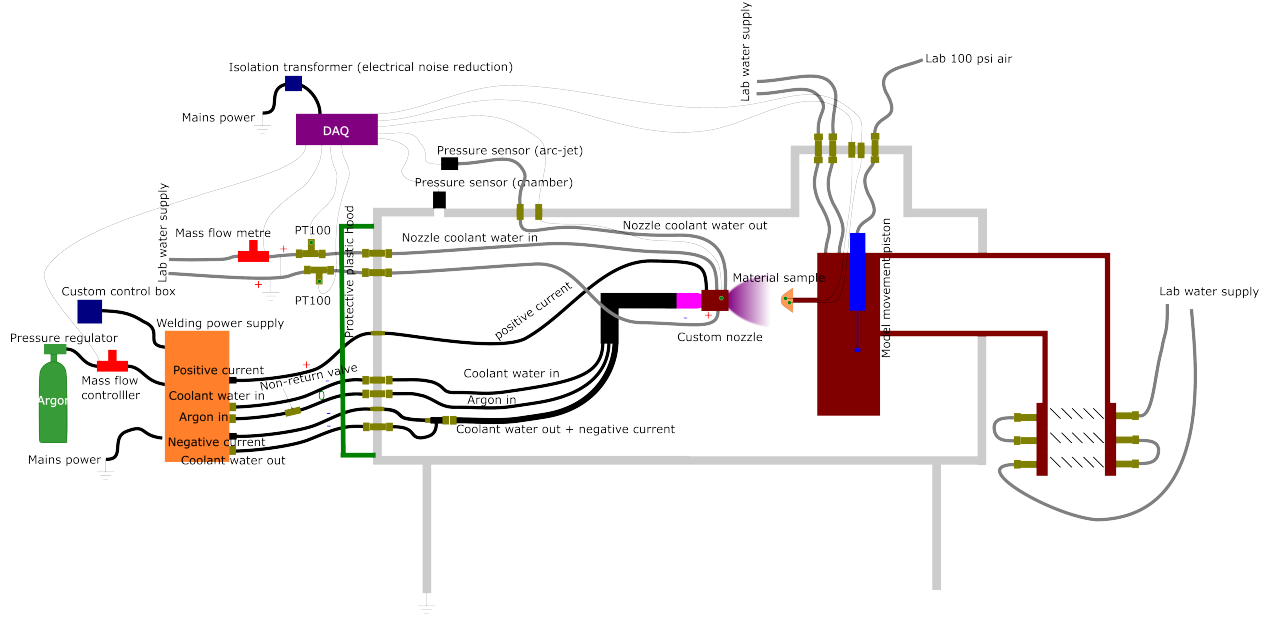


Fig. 1 Schematic of the OPG1 arcjet facility [32].

drives a 36 kg free-piston from the end of the piston launcher through a 9 m driver section, compressing the driver gas to high pressure and temperature. When the piston reaches the end of the driver tube, the high-pressure and temperature driver gas ruptures a 2.5 mm-thick steel diaphragm at ≈ 46.2 MPa. Rupturing the diaphragm generates a primary shock, propagating through the shock tube and compressing the test gas. When the primary shock bursts the secondary diaphragm, the test gas unsteadily expands through the low-pressure filled acceleration tube. This process further increases the total enthalpy and total pressure of the test gas behind the shock. Then, the test gas reaches the test section and generates a flow field around a test model.

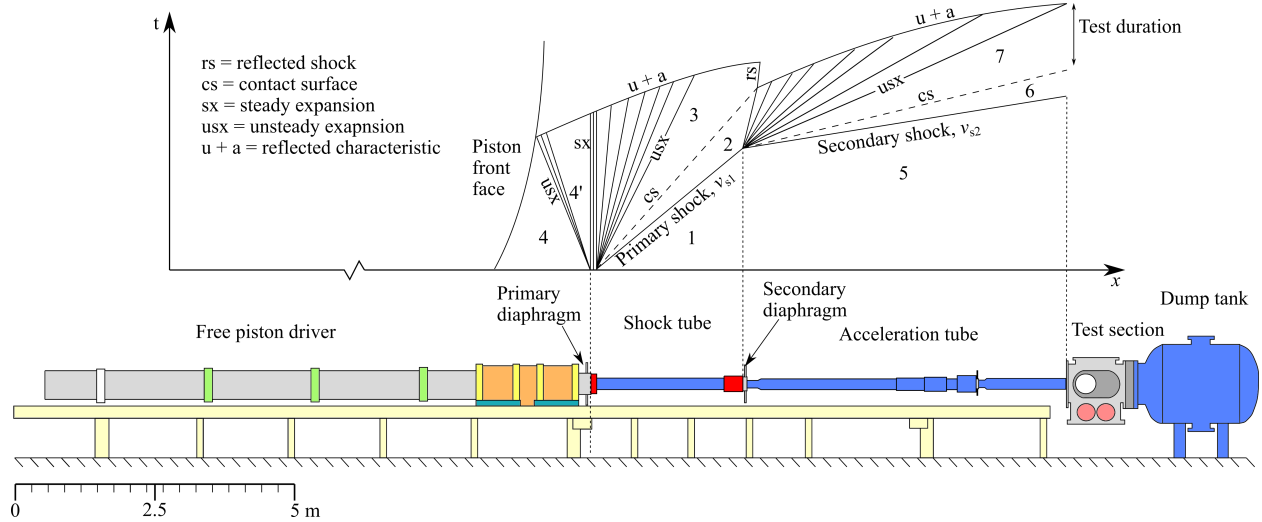


Fig. 2 Schematic of the T6 Stalker Tunnel: Expansion tube configuration [35].

For the future NASA Mars Sample Return (MSR) mission [38], the peak heating condition for the proposed MSR trajectory will experience a freestream density of $1.4 \times 10^{-3} \text{ kg/m}^3$, which is more than a magnitude higher than those for the previous sample return missions (i.e. Hayabusa or Stardust). This demands a higher performance in the expansion tube to drive a stronger shock through denser shock/expansion tubes. Also, a subscale model requires a much higher freestream density to retain density-length and binary scaling [39, 40]. Hence, new expansion tube conditions

were designed and tested to replicate the key representative trajectory points in flight. The PITOT [41] program was extensively used to determine the initial fill conditions. PITOT performs a theoretical chemical equilibrium state-to-state analysis of the expansion tube with a given set of parameters to estimate the facility properties. More details on flow design are discussed in our previous work [42].

Expansion tube experiments were performed with the initial fill conditions to check the feasibility of generating such flow conditions. Facility shock timing stations and the Pitot rake in the test section recorded piezoelectric pressure signals at different shock/expansion tube locations to characterise the flow condition. Using the pressure signals, shock speeds were calculated to determine freestream properties, which are summarised in Table 1. Two conditions named the *peak heating* and *nonequilibrium* conditions were developed, with the flight-equivalent velocity (U_∞ , calculated by $H_{t,flow} = U_\infty^2/2$) of 10.77 and 12.38 km/s, respectively. Fig. 3(a,b) shows the pressure traces of the 15° conehead probes [43] during the test. Time in the horizontal axis of the figures represents the time since the flow arrival at the conehead probe. After the flow startup, quasi-steady test-times (where we could confidently take the measurement) for both conditions were identified after the flow startup of the conehead probe when the pressure level reaches steady state, which maintain approximately 50 μ s. The averaged conehead probe pressure during the quasi-steady test-time (p_{cone}), which is the same as the horizontal line labelled PITOT, was used to adjust and infer the freestream properties. After the measurements are taken, the pressure continues to increase and terminates the quasi-steady test-time.

Table 1 T6 expansion tube flow properties [42].

Properties	Peak heating	Nonequilibrium
p_1 (kPa), measured	3.3	3.3
p_5 (Pa), measured	125	17
v_{s1} (m/s), measured	6575	6575
v_{s2} (m/s), measured	9524	11538
p_{cone} (kPa), measured	211.6	76.6
p_∞ (kPa), inferred	49.3	11.4
v_∞ (m/s), measured	9523	11538
ρ_∞ (kg/m ³), inferred	0.0243	0.00684
T_∞ (K), inferred	5533	4719
$H_{t,flow}$ (MJ/Kg), inferred	58.07	76.58
U_∞ (km/s), inferred	10.77	12.38

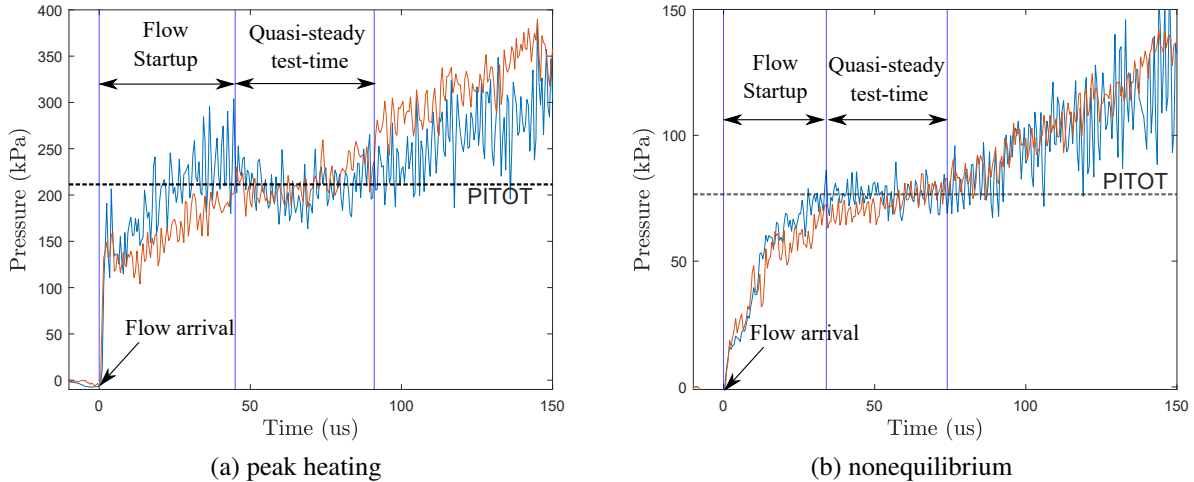


Fig. 3 Measured 15° conehead probe pressure traces for the new conditions [42].

B. Arc-jet Integration in the T6 Stalker Tunnel

Figure 4 illustrates the CAD representation of the OPG1 arc-jet integration in the T6 test section. The arc-jet is located above the expansion tube. The plasma heater box provides an extended volume to house connections and feedthroughs for electricity, gas, cooling-water, and pressure/temperature measurement of the arc-jet operation. The arc-jet is installed on a rail system with a stepper motor so that its streamwise (x) location can be adjusted to control the level of heating. From the arc-jet, the plasma flow generated will be argon for initial experiments but will be upgraded to provide nitrogen or air plasma in the future. In addition, the plasma flow will be enclosed by an exhaust channel to prevent the contamination/deposition of the ablated products inside the test section. The channel consists mainly of copper sheets for high thermal conductivity. Then, the plasma gas will flow through flexible bellows and vacuum flanges, evacuating outside of the test section. The model movement system is located downstream of the arc-jet, within the optical window access of the test section. When the arc-jet preheating is finished, the pneumatic actuator pushes down the model 200 mm vertically (y direction) from the centreline of the arc-jet to the exit of the expansion tube prior to a shot. When the tunnel is fired, a hypervelocity flow-field around an ablating test model is expected to be generated. This design generates a miniaturized plasma wind tunnel installed within the T6 test section. The only interface is a small opening through which the material sample will traverse just before the onset of expansion tube flow. This opening will be closed during the preheating process and only open as the test model is traversed. This method not only limits ablation contamination in the main test section but also enables a higher degree of pressure-decoupling between plasma channel flow and the T6 test section. Decoupled pressure in both parts of the facility allows for a wider range of flow conditions as the choice of p_5 (a significant expansion tube facility parameter) can be chosen somewhat independently from the pressure experienced in the plasma channel.

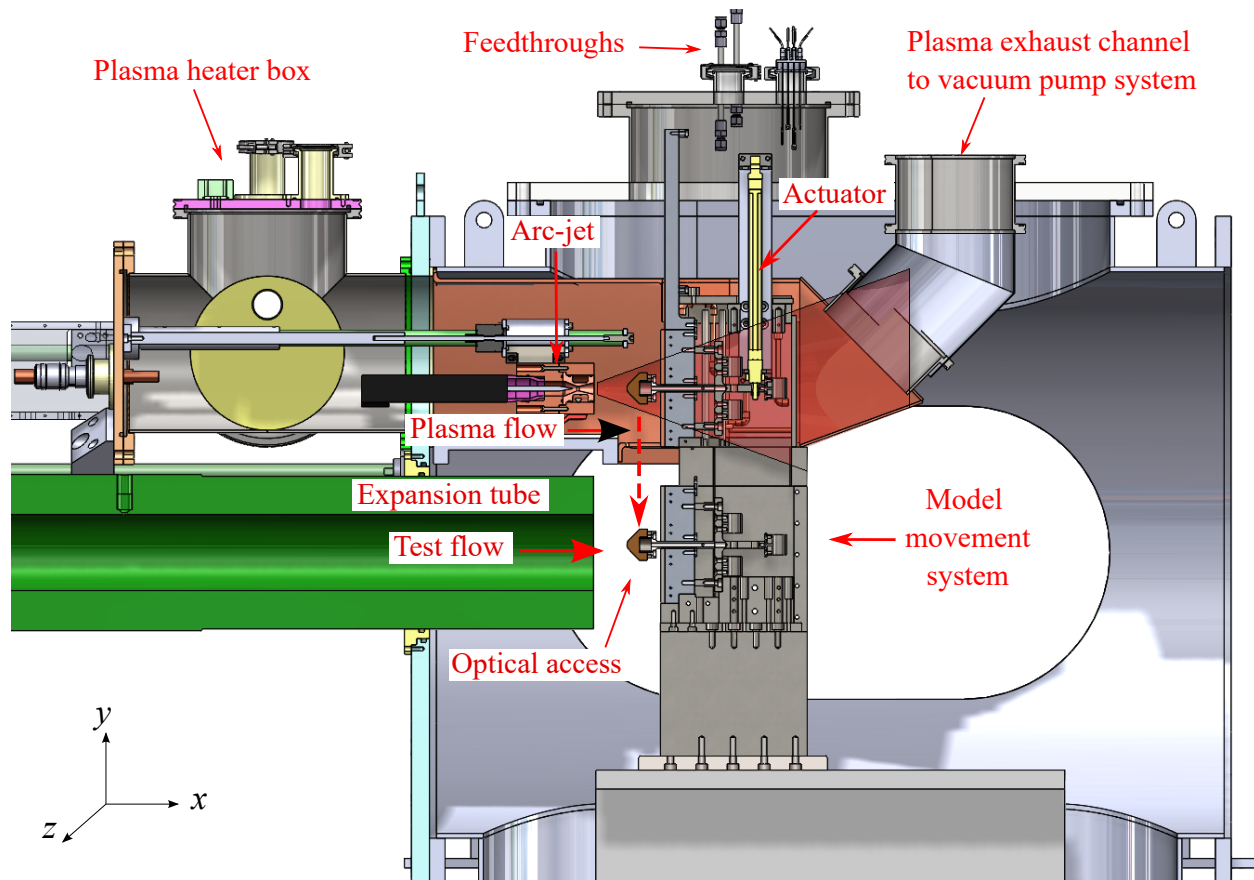


Fig. 4 Schematic of the arc-jet integration in the T6 test section.

C. Challenges of the Dual-Facility Preheating

Although the CAD representation in Fig. 4 could locate the critical components within the T6 test section, the dual-facility preheating concept has several major challenges. Figure 5 is a simplified schematic outlining the key parameters for the dual-facility experiment. First, a high vacuum performance of the plasma exhaust system is required to obtain desired test section/expansion tube pressure p_5 (125 Pa or 17 Pa for current work) before the shot. These pressures are crucial when generating desired shock speed and freestream condition [44]. Hence, an interplay between plasma and expansion tube conditions becomes vital as the MSR flow conditions require a high freestream density for model scaling. The mass flow rate of the arc-jet, \dot{m} , increases p_5 . This is aligned with a higher p_5 in the tunnel conditions, and less pumping power will be required for the vacuum exhaust system. Therefore, an established operating procedure is required to ensure a repeatable p_5 by fine-tuning the valve opening with the plasma operation. The infrastructure must be compatible between the two facilities, as the long-duration plasma generator requires water cooling with the rising temperature from high electrical current/power input. The impulse facility must have safety measures to isolate electricity and water from the facility test section, as their leaks could damage the tunnel infrastructure. Moreover, a proper synchronisation between the arc-jet and the expansion tube needs to be carefully considered to ensure the effective and safe operation of the expansion tube.

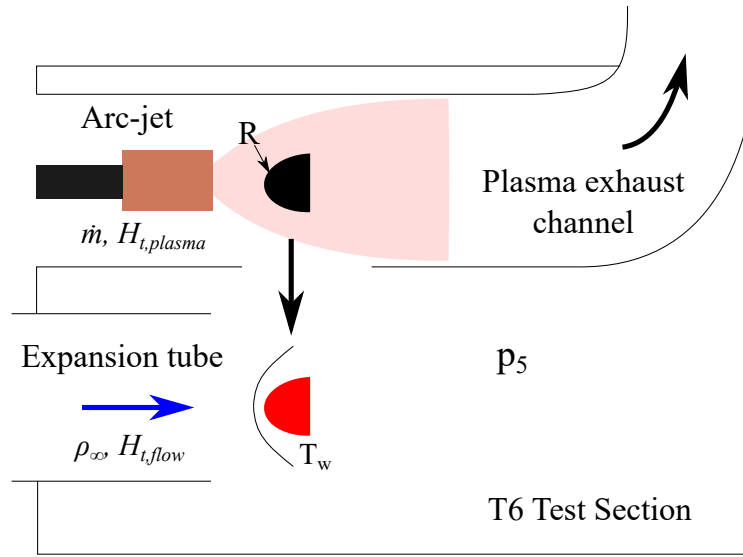


Fig. 5 Key parameters for the dual-facility preheating experiment.

A single-use sphere-cone test model should be easily replaced after the preheating tests to save time for a turnaround. The position of the model must be accurate to ensure the repeatability of tests after the replacement. The heat flux as a function of the model scale needs to be matched to achieve the right heat flux on the plasma side and the right density-length scaling in the hypersonic flow. For the current setup, the size of the test model is determined by the size of the arc-jet and its maximum electrical power. In a rigorous experimental simulation, the arc-jet needs much higher electrical power to match the total enthalpy of the expansion tube flow ($H_{t,plasma} = H_{t,flow} = 58 \text{ MJ/kg}$ or 76.6 MJ/kg). The smaller size of the model is advantageous with smaller nose radius R will reach higher T_w for ablation. For density-length scaling, however, a smaller size requires a much higher freestream density (ρ_∞) to properly match binary scaling in expansion tube flows [39, 40]. The density is limited by the performance of the impulse facility. A smaller model is also challenging from the optical diagnostic perspective because its thin shock layer requires a much higher magnification in setting up the line-of-sight emission spectroscopy.

The model movement system must survive both the long-duration arc-jet heating and the high total pressures/diaphragm debris impact of the expansion tube flow. Therefore, a high temperature/high tensile strength material must be used to accommodate the extreme environment. Although the two facilities are effectively decoupled when serving their purpose, the part of the model system where it gets exposed to both facilities, for example, the leading edge of the model, needs to withstand the heat flux during plasma heating and the pressure load of the expansion tube flow. A sharp radius for the leading edge of the model is advantageous for expansion tube flow (oblique shock reducing forces) but for plasma heating (high heat flux at the leading edge due to small nose radius). A larger radius in

the expansion tube flow will create a detached bow shock leading to higher pressure loads. Within the model movement system, the test model assembly must also traverse quickly in a vertical direction when the system is triggered. Also, when the model faces the flow, it must have minimal movement during the steady test-time of the expansion tube flow, which is also important for the alignment of optical diagnostics.

If these challenges in dual-facility integration are addressed, the plasma preheating could provide a comprehensive prospect in experimental hypersonic testing. Firstly, compared with resistive Ohmic heating, plasma heating does not require any electric current to flow within a heated section of the test model. This allows greater flexibility in testing any material with axisymmetric or complex/realistic model geometries. The heated sample does not have to be electrically conductive and possesses high electrical resistivity to reach higher surface temperatures. Secondly, the plasma heating can provide surface heating rather than volumetric heating, which allows closer replication of high-temperature physics encountered in flight, such as pyrolysis and spallation [45]. If the total enthalpy of the air plasma is matched with the test flow, the dual-facility preheating experiments with realistic test models become more representative of actual re-entry flight.

D. Flow Diagnostics

Figure 6 schematically shows the flow diagnostics to be used in the experiments. During the plasma heating, surface temperature distribution of the preheated model will be captured by an Optris P1 M infrared camera and a point-measurement will be captured by a fibre-coupled spectrometer. The temperature of the model could also be indirectly monitored by several in-situ thermocouples which are installed opposite of the ablating surface. When the tunnel is fired, a high-speed camera with an atomic oxygen filter will record the flow-field development of the preheated model. Along with the high-speed camera, two spectrographs, each representing red and ultraviolet wavelength regions, will be positioned in the side ports to capture the spectra during steady test-time. A telecentric optical path will be adapted to minimise the spatial blur due to ray divergence [46]. In addition to the non-intrusive methods, a 15° conehead pressure probe will be positioned next to the test model (within the core-flow, but the shock angle not interfering with the model) to serve as a reference gauge to infer the freestream pressure.

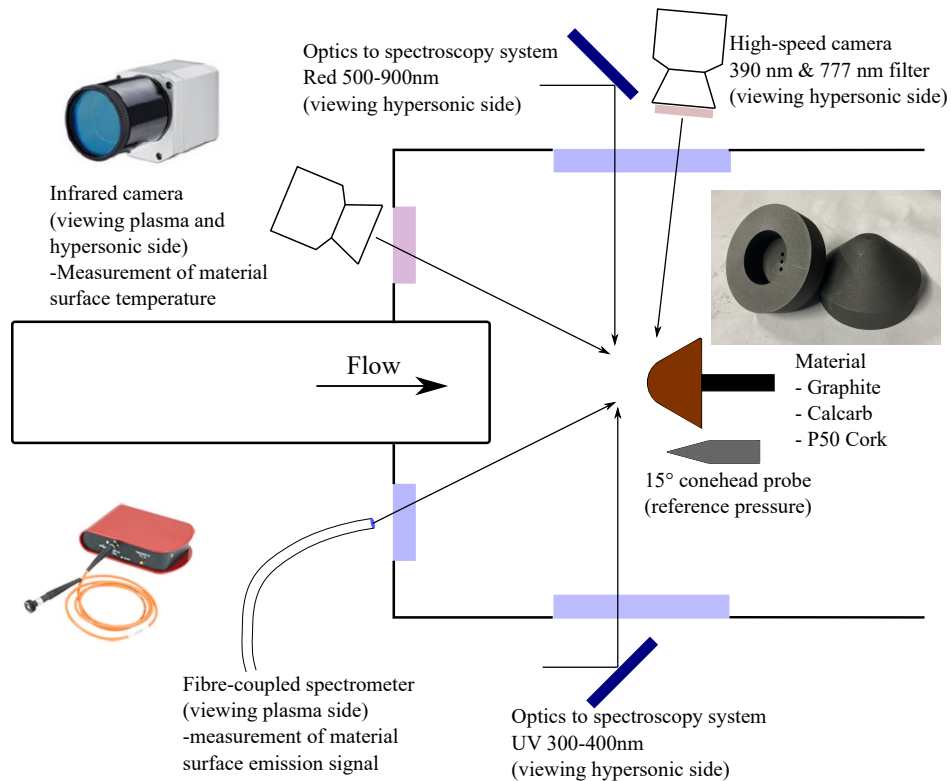


Fig. 6 Overview of the experimental flow diagnostics.

E. Model Movement System

The model movement system in Fig. 4 must traverse the preheated model to the exit of the expansion tube. Fig. 7 shows the illustration of the three major sub-assemblies of the model movement system. The test model in Fig. 7(a) consists of a 40 mm diameter sphere cone representing the notional MSR EEV capsule geometry [38] and a cross beam structure. The capsule model is a 45° sphere-cone geometry with a nose radius of 9 mm. The materials are P50 cork, Calcarb and Graphite for the initial testing. P50 has been used as heat-shield material for re-entry vehicles [47], Calcarb as a charred carbon fibre structure [6] and graphite could be tested as a solid, non-ablating comparison. When the plasma heating is finished, the pneumatic actuator moves the heated model from the plasma source to the expansion tube. The test model is on rail, bounded by two vertical shafts. The traverse methodology was adapted from the free-flight model drop mechanism in the reference [48]. Then, both the test model and model movement support get directly exposed to the hypersonic flow from the expansion tube. The leading edge behind the test model was kept at a sharp angle (20°) to avoid facility unstart. The model movement support in Fig. 7(b) aims to: i) shield the moving test model assembly and ii) fix the location in the tunnel. EN-24T (34CrNiMo6) was chosen as the primary material to guarantee maximum material strength. The plasma protection support assembly in Fig. 7(c) is assembled above the model movement support. The plasma support houses a pneumatic actuator, also protected from the hot plasma gas using copper shields. This assembly is located outside the core-flow of the tunnel, so no significant pressure loads from the test flow are expected or diaphragm debris. The following section will provide numerical results for flow-field, heat transfer, and structural analysis on the critical parts of the model movement system.

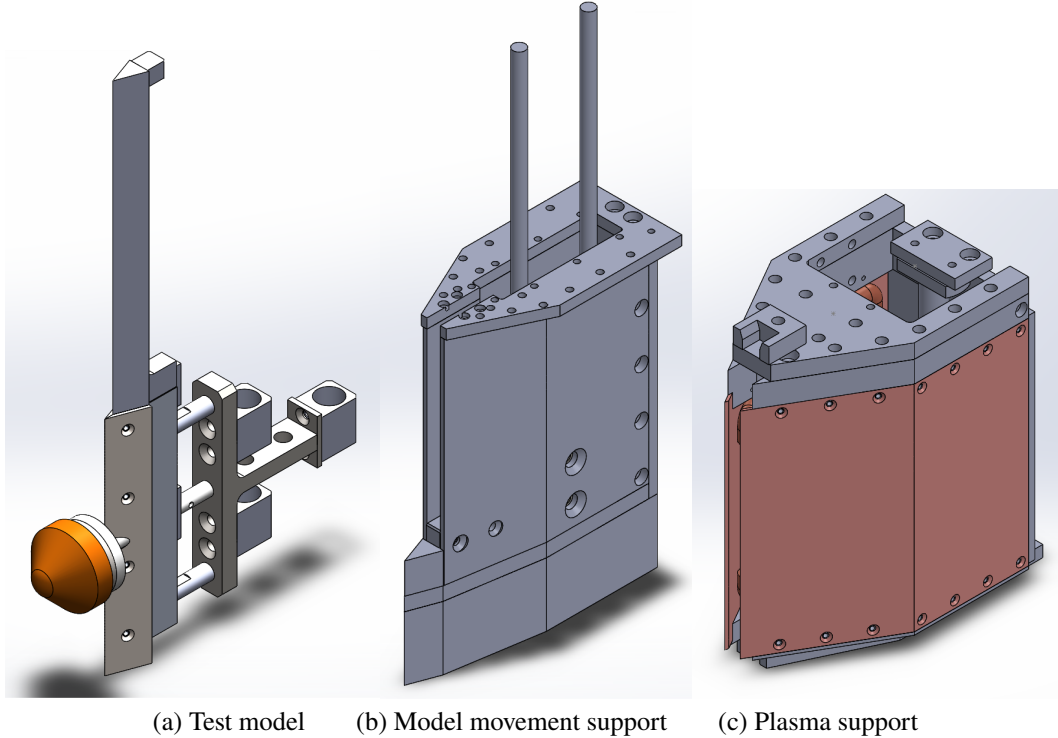


Fig. 7 Sub-components of the model movement system.

V. System Design Analysis

A. Plasma Flow-field Analysis

First, the flow-field around the plasma support structure (leading edge and plasma channel) was simulated by the multiphysics tool COMSOL [49]. A COMSOL Computational Fluid Dynamics (CFD) module was used, using the expected plasma flow conditions listed in Table 2. Physical and computational domains for CFD are illustrated in Fig. 8(a,b). The solid walls of the mounting structure consists of the leading edge W and shielding plates A , B and

C, which are labelled as dark blue lines with four stations (1,2,3,4) in the computational domain. Fig. 9 shows the calculated surface properties along the stations 1 to 4. The boundary-layer edge velocity plot in Fig. 9(a) shows that the flow is decelerated at station 2 as it is compressed at the elbow and accelerates at station 3 as it expands around the corner. At the same time, both temperature and pressure distribution in Fig. 9(b) decreases until station 3, yet these values increase as it expands at station 4. Overall, the calculated temperature and pressures vary about 100 K and 2kPa from the p_t and T_t , respectively.

Table 2 Argon flow condition at the plasma torch exit [25]

Properties	Value
\dot{m} (g/s)	0.2
M	0.2
v (m/s)	226.75
$T_{t,plasma}$ (K)	3750
$p_{t,plasma}$ (mbar)	550
$H_{t,plasma}$ (MJ/Kg)	11.2

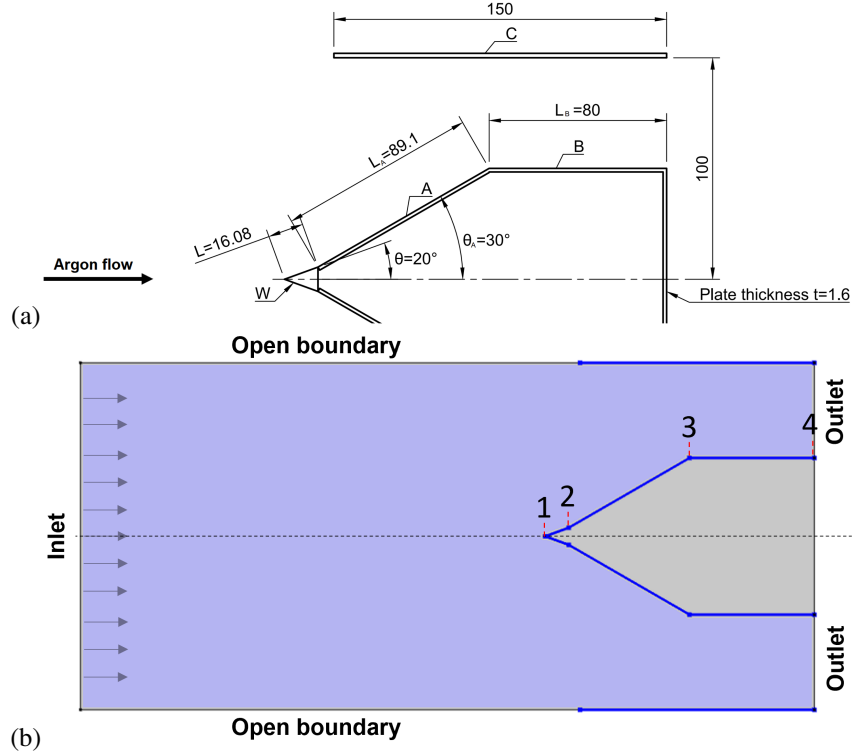


Fig. 8 Plasma support structure: (a) top-view, dimensions in mm. (b) computational domain.

B. Heat Transfer Analysis

Next, a COMSOL heat transfer module examined the heat transfer on the leading edge after 100s of preheating by using the boundary-layer edge properties calculated in Fig. 9. An example temperature distribution is plotted in Fig. 10. The region closest to the leading edge is the hottest due to the high heat flux at the nearest surfaces and the smaller mass locally. For the leading-edge design, the maximum temperature reached during preheating must be below the melting temperature of the copper (1358K). Fig. 11 shows the results for a parametric study where the leading edge length and angle have been varied. The dashed red line is the 1358 K isotherm and the dotted blue line indicates the

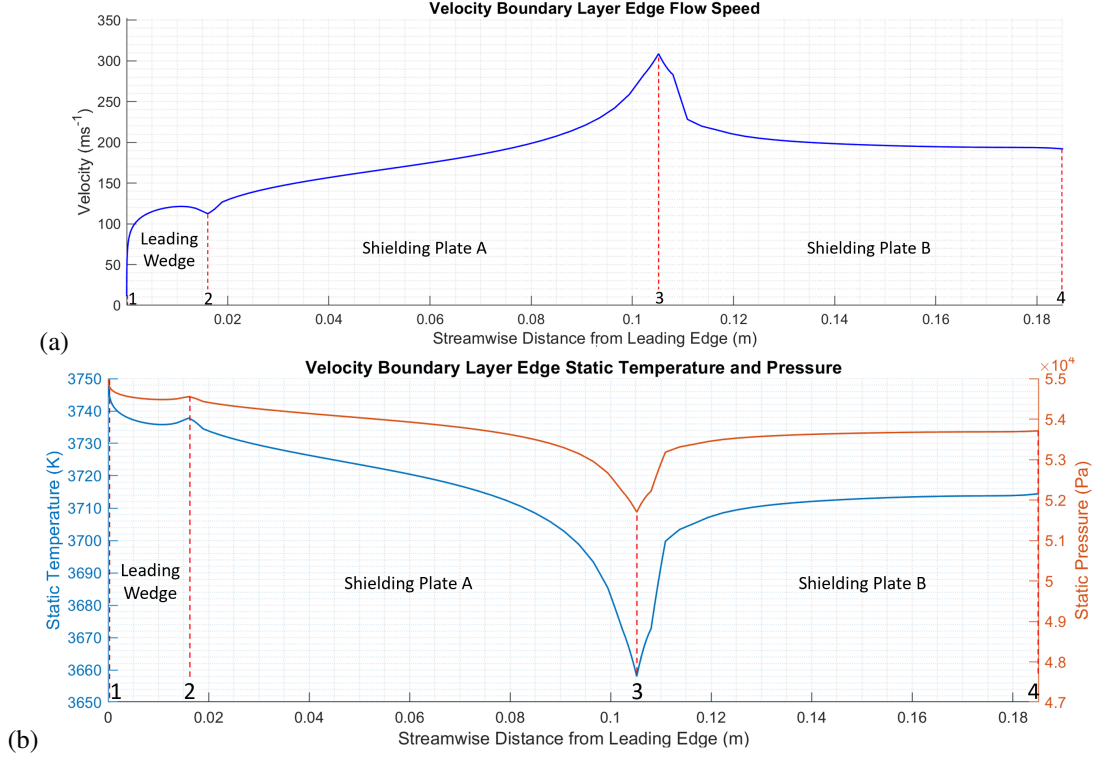


Fig. 9 Boundary-layer edge flow properties over the plasma support structure.

1358 K isotherm for the averaged temperature. The contour plot shows that the red line and arrow direction gives the feasible region without water-cooling. For the current design, the leading-edge angle is 20° with a streamwise distance of 24 cm. Although this means it will be located between the red and the dotted blue line, the ablating test model will decrease the energy of the plasma before reaching to the leading edge. Future adaptations to the leading edge will include water-cooling to allow for higher enthalpy plasma flow conditions.

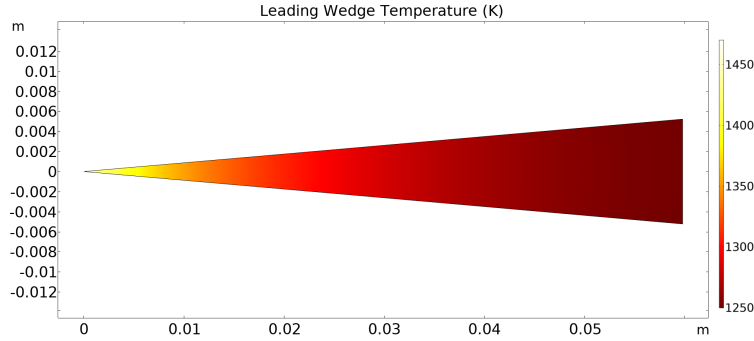


Fig. 10 Sample temperature distribution in the leading edge cross-section ($\theta = 5^\circ$, $L = 60\text{mm}$)

C. Structural Analysis

The model movement system must withstand the pressure loads of the T6 test flow. In an expansion tube configuration, the maximum loads occur after the test time with the driver gas arrival [15], often damaging the test article in the test section. The pressure loads at each section of the model movement support were determined by using the pressure and Mach number of the driver gas (p_1 and M_1). The values are labelled in Fig. 12, where p_2 , p_3 , p_4 , and p_{pitot} were calculated by using ideal shock/expansion wave relations, which were then applied as pressure loads in the finite-element

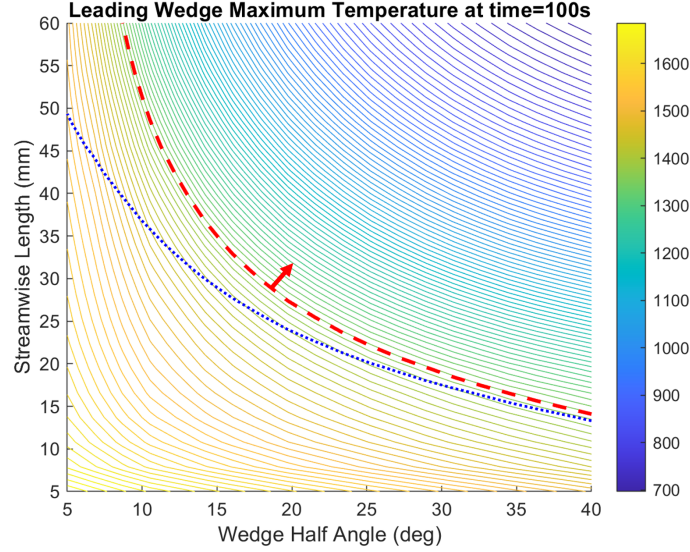


Fig. 11 Parametric contour plot for maximum leading edge temperature after 100s.

structural simulations.

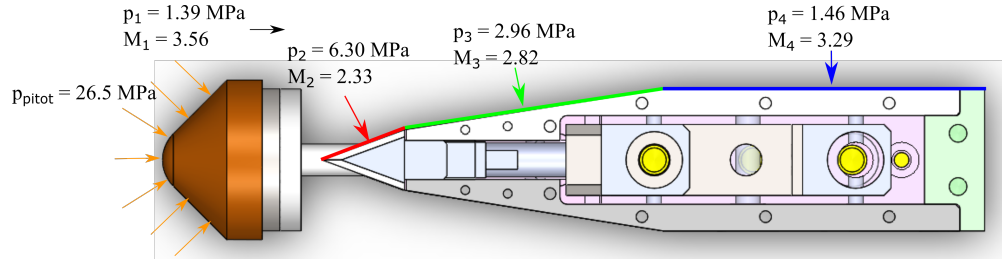


Fig. 12 Pressure loads applied to the model movement system using state 3, top-view.

For the load analysis, a finite element analysis module in Solidworks [50] was used. A curvature-based mesh with the finest density (Fig. 13(a)) was constructed for the model movement geometry. The mesh has 202406 nodes and 114484 elements. To accommodate the size of the T6 core flow (60 mm diameter), the loads calculated in Fig. 12, are only applied to the model movement support section, region within the red circle, as a conservative estimate. A fixed geometry boundary condition is applied to the bottom face of the assembly as it will be bolted and fixed onto the T6 test section. A perfect fit between the parts (e.g. leading edge block and side plate) was assumed throughout. Figure 13(b) shows the deformation distribution from the finite element analysis. The maximum deformation expected is only 0.16 mm in the middle of the plot. This maximum deformation is also reflected in the Factor of Safety (FOS) distributions of Fig. 13(c,d). The FOS is much higher than one throughout the model system. Looking into the inner side in Fig. 13(d), there are local regions with smaller FOS (close to 1). However, there will not be any significant deformation of the model, especially considering the very short time duration of the load. Note that the material for the capsule model is also EN-24T. Therefore, if the P50 cork or Graphite is used as a preheated material sample - the capsule model is not likely to survive after a shot. The load analysis ensures that the model movement system will be safe for the test duration during a T6 shot.

VI. Conclusion

This paper provided a conceptual design of integrating an arc-jet in the T6 Stalker Tunnel to realise experimental investigation of hypervelocity flow over an ablating test model. A small-scale arc-jet OPG1 will be installed in the T6 test section, serving as a preheating device to ablate the test model. Then, the model will traverse vertically to position within the expansion tube core-flow. A recent T6 expansion tube test campaign highlighted that the T6 could

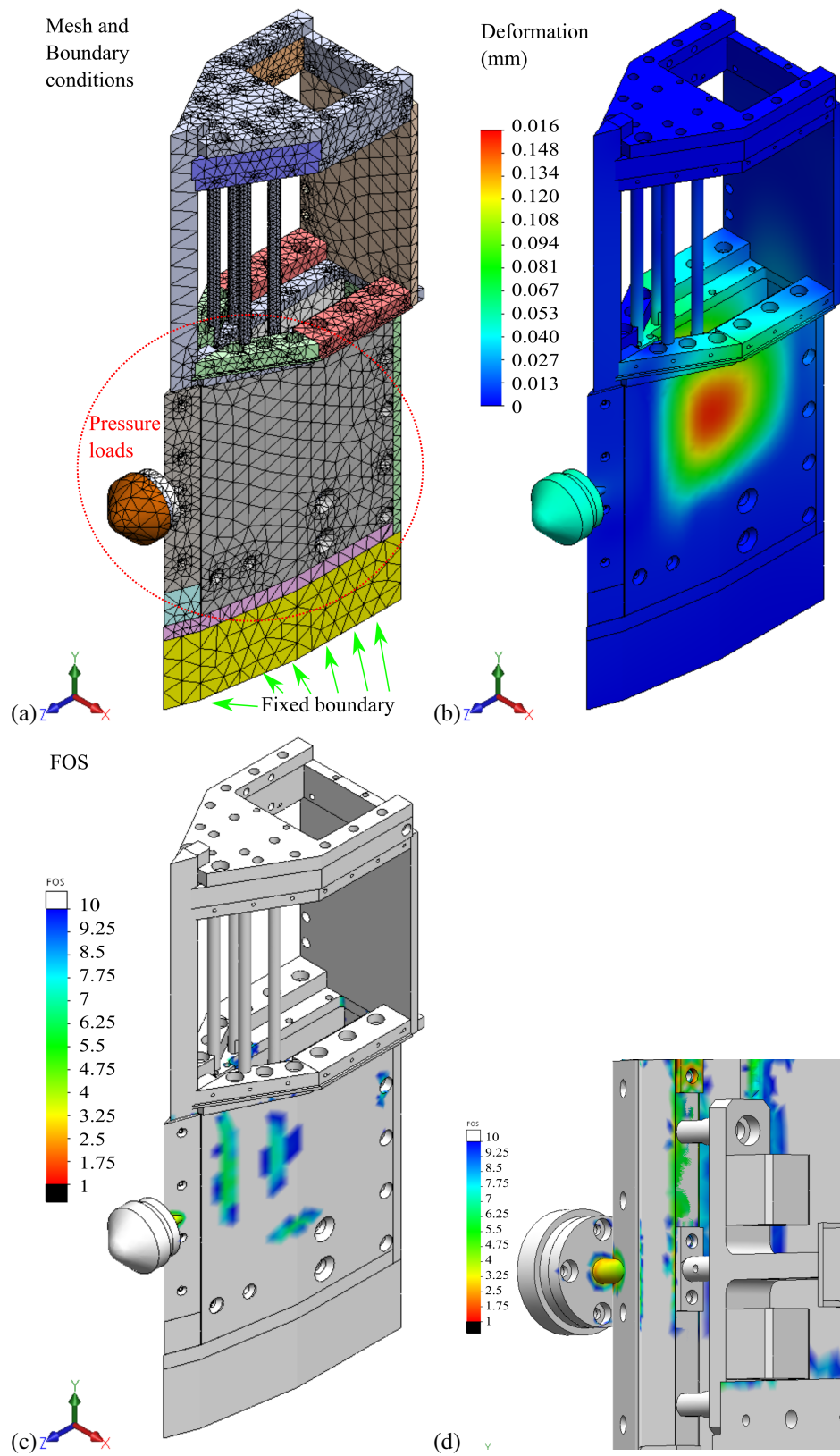


Fig. 13 Finite element analysis of the model movement system.

generate hypervelocity flows representative of future Mars Sample Return mission trajectories. The flow conditions matched the total enthalpies with the highest possible density. Next, the major engineering challenges of the dual-facility setup were outlined in detail. With the current design, preliminary thermal and structural analyses were conducted on the movement system using plasma and expansion tube flow conditions, respectively. The studies indicated that the design would be feasible for the experiment. When these challenges are properly addressed, the dual-facility preheating could become a benchmark methodology for combining essential flow features of a hypersonic re-entry flow environment. Further validation and analysis of the proposed methodology are currently being conducted in addition to developing a dual-facility setup. These include a detailed design of the apparatus and the benchtop testing of the model movement system. Commissioning the OPG1 plasma wind tunnel is expected to occur in the first half of 2023, aiming to characterise the argon plasma and the heated test model with the vacuum performance.

Acknowledgments

This research was funded by the UKRI Future Leaders Fellowship scheme (grant number MR/T041269/1), and we extend our gratitude to UKRI. For Open Access, the author has applied a CC BY public copyright licence to any Author Accepted Manuscript (AAM) version arising from this submission. We appreciate Christopher Johnston of NASA for sharing the flow conditions of the Mars Sample Return mission trajectory points and the capsule model geometry. We also thank Chris Hambidge and Luke Doherty for discussing the concept design and providing insights on the arc-jet integration.

References

- [1] Park, C., "Review of chemical-kinetic problems of future NASA missions. I-Earth entries," *Journal of Thermophysics and Heat transfer*, Vol. 7, No. 3, 1993, pp. 385–398. <https://doi.org/10.2514/3.431>.
- [2] Johnston, C. O., Mazaheri, A., Gnoffo, P., Kleb, B., and Bose, D., "Radiative Heating Uncertainty for Hyperbolic Earth Entry, Part 1: Flight Simulation Modeling and Uncertainty," *Journal of Thermophysics and Heat Transfer*, Vol. 50, No. 1, 2013, pp. 19–38. <https://doi.org/10.2514/1.A32254>.
- [3] Johnston, C. O., Sutton, K., Prabhu, D., and Bose, D., "Radiative Heating Uncertainty for Hyperbolic Earth Entry, Part 2: Comparisons with 1960s-Era Shock-Tube Measurements," *Journal of Thermophysics and Heat Transfer*, Vol. 50, No. 1, 2013, pp. 39–47. <https://doi.org/10.2514/1.A32483>.
- [4] Johnston, C. O., Brandis, A. M., and Bose, D., "Radiative Heating Uncertainty for Hyperbolic Earth Entry, Part 3: Comparisons with Electric Arc Shock-Tube Measurements," *Journal of Thermophysics and Heat Transfer*, Vol. 50, No. 1, 2013, pp. 48–55. <https://doi.org/10.2514/1.A32484>.
- [5] Hermann, T., Löhle, S., Wei, H., Morgan, R., Bauder, U., and Fasoulas, S., "Quantitative Emission Spectroscopy for Superorbital Re-entry in the Expansion Tube X2," *Journal of Thermophysics and Heat Transfer*, Vol. 31, No. 3, 2017, pp. 257–268. <https://doi.org/10.2514/1.T4898>.
- [6] Hermann, T., Löhle, S., Fasoulas, S., Leyland, P., Marraffa, L., and Bouilly, J.-M., "Influence of Ablation on Vacuum-Ultraviolet Radiation in a Plasma Wind Tunnel Flow," *Journal of Thermophysics and Heat Transfer*, Vol. 31, No. 3, 2017, pp. 575–585. <https://doi.org/10.2514/1.T4936>.
- [7] Lu, F. K., and Marren, D. E., *Advanced hypersonic test facilities*, Vol. 198, American Institute of Aeronautics and Astronautics, 2002. <https://doi.org/https://doi.org/10.2514/4.866678>.
- [8] Auweter-Kurtz, K. H. L., Monika, and Laure, S., "Plasma Generators for Re-Entry Simulation," *Journal of Propulsion and Power*, Vol. 12, No. 6, 1996, pp. 1053–1061. <https://doi.org/10.2514/3.24143>.
- [9] Balter-Peterson, A., Nichols, F., Mifsud, B., and Wednell, L., "Arc jet testing in NASA Ames Research Center thermophysics facilities," *AIAA 4th International Aerospace Planes Conference*, American Institute of Aeronautics and Astronautics, 1992. <https://doi.org/10.2514/6.1992-5041>.
- [10] Caristia, S., De Filippis, F., Del Vecchio, A., and Graps, E., "SCIROCCO PWT facility for high temperature material assembly testing," *54th International Astronautical Congress*, 2003. <https://doi.org/10.2514/6.IAC-03-I.3.04>.
- [11] MacDonald, M. E., Jacobs, C. M., Laux, C. O., Zander, F., and Morgan, R. G., "Measurements of Air Plasma/Ablator Interactions in an Inductively Coupled Plasma Torch," *Journal of Thermophysics and Heat Transfer*, Vol. 29, No. 1, 2014, pp. 12–23. <https://doi.org/10.2514/1.T4402>.

- [12] Löhle, S., Zander, F., Eberhart, M., Hermann, T., Meindl, A., Massuti-Ballester, B., Leiser, D., Hufgard, F., Pagan, A. S., Herdrich, G., and Fasoulas, S., "Assessment of high enthalpy flow conditions for re-entry aerothermodynamics in the plasma wind tunnel facilities at IRS," *CEAS Space Journal*, Vol. 14, 2021, pp. 1–12. <https://doi.org/10.1007/s12567-021-00396-y>.
- [13] Kolesnikov, A. F., "Extrapolation from High Enthalpy Tests to Flight Based on the Concept of Local Heat Transfer Simulation," Tech. Rep. RTO-EN-8, 2000. URL <https://apps.dtic.mil/sti/pdfs/ADP010749.pdf>.
- [14] Stalker, R. J., Paull, A., Mee, D. J., Morgan, R. G., and Jacobs, P. A., "Scramjets and Shock Tunnels - The Queensland Experience," *Progress in Aerospace Sciences*, Vol. 41, No. 6, 2005, pp. 471 – 513. <https://doi.org/10.1016/j.paerosci.2005.08.002>.
- [15] Gildfind, D. E., Morgan, R. G., and Jacobs, P. A., "Expansion Tubes in Australia," *Experimental Methods of Shock Wave Research*, edited by O. Igra and F. Seiler, Springer-Verlag, 2016, pp. 399–431. https://doi.org/10.1007/978-3-319-23745-9_13.
- [16] Zander, F., Morgan, R. G., Sheikh, U., Buttsworth, D. R., and Teakle, P. R., "Hot-wall Reentry Testing in Hypersonic Impulse Facilities," *AIAA Journal*, Vol. 51, No. 2, 2013, pp. 476–484. <https://doi.org/10.2514/1.J051867>.
- [17] Lewis, S. W., Morgan, R. G., McIntyre, T. J., Alba, C. R., and Greendyke, R. B., "Expansion Tunnel Experiments of Earth Reentry Flow with Surface Ablation," *Journal of Spacecraft and Rockets*, Vol. 53, No. 5, 2016, pp. 887–899. <https://doi.org/10.2514/1.A33267>.
- [18] Lewis, S. W., James, C. M., Ravichandran, R., Morgan, R. G., and McIntyre, T. J., "Carbon Ablation in Hypervelocity Air and Nitrogen Shock Layers," *Journal of Thermophysics and Heat Transfer*, Vol. 32, No. 2, 2018, pp. 449–468. <https://doi.org/10.2514/1.T5270>.
- [19] Ravichandran, R., Buttsworth, D. R., Lewis, S. W., Morgan, R. G., and McIntyre, T. J., "Filtered Image Thermography for High Temperatures in Hypersonic Preheated Ablation Experiments," *Journal of Thermophysics and Heat Transfer*, Vol. 33, 2019, pp. 1074–1084. <https://doi.org/10.2514/1.T5629>.
- [20] Ravichandran, R., Buttsworth, D. R., Lewis, S. W., Morgan, R. G., and McIntyre, T. J., "Graphite Ablation and Radiation on Interaction with Hypervelocity Earth-Entry Flows," *Journal of Thermophysics and Heat Transfer*, Vol. 35, 2021, pp. 335–348. <https://doi.org/10.2514/1.T5928>.
- [21] Iyinomen, D. O., Malpress, R., and Buttsworth, D., "Technique Development for Investigating Axisymmetric Ablation Models in Hypersonic Impulse Facilities," *AIAA Journal*, Vol. 59, No. 6, 2021, pp. 1899–1913. <https://doi.org/10.2514/1.J059629>.
- [22] Chang, E. W. K., Chan, W. Y. K., Hopkins, K. J., McIntyre, T. J., and Veeraragavan, A., "Electrically-heated flat plate testing in a free-piston driven shock tunnel," *Aerospace Science and Technology*, Vol. 102, 2020, pp. 1–11. <https://doi.org/10.1016/j.ast.2020.105856>.
- [23] Chang, E. W. K., Chan, W. Y. K., McIntyre, T. J., and Veeraragavan, A., "Hypersonic shock impingement on a heated flat plate at Mach 7 flight enthalpy," *Journal of Fluid Mechanics*, Vol. 908, 2021, pp. 1–13. <https://doi.org/10.1017/jfm.2020.877>.
- [24] Chang, E. W. K., Chan, W. Y. K., McIntyre, T. J., and Veeraragavan, A., "Hypersonic shock impingement studies on a flat plate: flow separation of laminar boundary layers," *Journal of Fluid Mechanics*, Vol. 951, No. A19, 2022, pp. 1–27. <https://doi.org/10.1017/jfm.2022.827>.
- [25] Peichl, J., "Characterization of a miniature arcjet heater," Ph.D. thesis, Institute of Space Systems, University of Stuttgart, 2019.
- [26] Böhrk, H., and Jemmali, R., "Time resolved quantitative imaging of charring in materials at temperatures above 1000K," *Review of Scientific Instruments*, Vol. 87, No. 073701, 2016. <https://doi.org/10.1063/1.4955441>.
- [27] Nawaz, A., Ho, T. S., Philippidis, D., MacDonald, M., McGlaughlin, M. S., and Driver, D. M., "Baseline characterization of the 30kW miniature arc jet facility mARC at NASA Ames," AIAA AVIATION Forum, American Institute of Aeronautics and Astronautics, 2016. <https://doi.org/10.2514/6.2016-3819>.
- [28] MacDonald, M. E., Philippidis, D., Ho, T. S., Haw, M., Hartman, J., and McGlaughlin, M., "Build-up of the second-generation 30 kW miniature arc jet (mARC II) at NASA Ames Research Center," *AIAA Aviation 2019 Forum*, American Institute of Aeronautics and Astronautics, 2019. <https://doi.org/10.2514/6.2019-2857>.
- [29] Noh, S., and Kim, K. H., "Estimation of Tungsten Ablation Test Conditions Using 150 Kilowatt Arc Heater," *Journal of Thermophysics and Heat Transfer*, Vol. 35, 2019, pp. 1096–1111. <https://doi.org/10.2514/1.T5693>.
- [30] Luís, D., and MacDonald, M. E., "Emission spectroscopy characterization of electrode species in the freestream flow at the NASA Ames miniature Arc Jet II facility," *Journal of Quantitative Spectroscopy and Radiative Transfer*, Vol. 272, 2021, pp. 1–12. <https://doi.org/10.1016/j.jqsrt.2021.107752>.

- [31] Mundt, C., “Development of the New Piston-Driven Shock-Tunnel HELM,” *Experimental Methods of Shock Wave Research*, edited by O. Igra and F. Seiler, Springer International Publishing, Cham, 2016, pp. 265–283. https://doi.org/10.1007/978-3-319-23745-9_8.
- [32] Hermann, T. A., Chang, E. W. K., Schäfer, J., Joglekar, C., and Böhrk, H., “Development of Small Scale Arc-jet Facility OPG1,” *AIAA SciTech 2023 Forum*, 2023, pp. 1–24.
- [33] McGilvray, M., Doherty, L. J., Morgan, R. G., Gildfind, D. E., Jacobs, P., and Ireland, P., “T6: The Oxford University Stalker Tunnel,” *20th AIAA International Space Planes and Hypersonic Systems and Technologies Conference*, 2015, pp. 1–11. <https://doi.org/10.2514/6.2015-3545>.
- [34] Collen, P. L., Doherty, L. J., Subiah, S. D., Sopek, T., Jahn, I., Gildfind, D., Penty-Garaets, R., Gollan, R., Hambidge, C., Morgan, R. G., and M., M., “Development and Commissioning of the T6 Stalker Tunnel,” *Experiments in Fluids*, Vol. 62, No. 225, 2021. <https://doi.org/10.1007/s00348-021-03298-1>.
- [35] Steer, J., Collen, P. L., Glenn, A., Sopek, T., Hambidge, C., Doherty, L., McGilvray, M., Löhle, S., and Walpot, L., “Experimental Study of a Galileo Sub-Scale Model at Ice Giant Entry Conditions in the T6 Free-Piston Driven Wind Tunnel,” *AIAA SciTech 2023 Forum*, 2023.
- [36] Glenn, A. B., Collen, P. L., and McGilvray, M., “Experimental Non-Equilibrium Radiation Measurements for Low-Earth Orbit Return,” *AIAA SCITECH 2022 Forum*, American Institute of Aeronautics and Astronautics, 2019. <https://doi.org/10.2514/6.2022-2154>.
- [37] Collen, P. L., Satchell, M., Di Mare, L., and M., M., “The influence of shock speed variation on radiation and thermochemistry experiments in shock tubes,” *Journal of Fluid Mechanics*, Vol. 948, No. A51, 2022. <https://doi.org/10.1017/jfm.2022.727>.
- [38] Johnston, C., “personal communication,” , 2019.
- [39] de Crombrughe, G., Morgan, R. G., and Chazot, O., “Theoretical approach and experimental verification of the role of diffusive transport under binary scaling conditions,” *International Journal of Heat and Mass Transfer*, Vol. 97, 2016, pp. 675–682. <https://doi.org/10.1016/j.ijheatmasstransfer.2016.02.018>.
- [40] de Crombrughe, G., Chazot, O., McIntyre, T. J., and Morgan, R. G., “Experimental evidence of the impact of radiation coupling on binary scaling applied to shock layer flows,” *International Journal of Heat and Mass Transfer*, Vol. 120, 2018, pp. 568–574. <https://doi.org/10.1016/j.ijheatmasstransfer.2017.12.071>.
- [41] James, C. M., Gilfind, D., Lewis, S. W., Morgan, R. G., and Zander, F., “Implementation of a state-to-state analytical framework for the calculation of expansion tube flow properties,” *Experiments in Fluids*, Vol. 28, No. 2, 2018, pp. 349–377. <https://doi.org/10.1007/s00193-017-0763-3>.
- [42] Chang, E. W. K., Hermann, T. A., Collen, P. L., McGilvray, M., and James, C. M., “Mars Sample Return Condition Design and Testing in T6 Stalker Tunnel,” *9th International Workshop on Radiation of High Temperature Gases for Space Missions*, 2022.
- [43] McGilvray, M., Jacobs, P. A., Morgan, R. G., Gollan, R. J., and Jacobs, C. M., “Helmholtz Resonance of Pitot Pressure Measurements in Impulsive Hypersonic Test Facilities,” *AIAA Journal*, Vol. 47, No. 10, 2009, pp. 2430–2439. <https://doi.org/10.2514/1.42543>.
- [44] James, C. M., Lewis, S. W., Morgan, R. G., Liu, Y., and Lefevre, A., “Generating High-Speed Earth Reentry Test Conditions in an Expansion Tube,” *Journal of Spacecraft and Rockets*, Vol. 58, No. 2, 2021, pp. 345–362. <https://doi.org/10.2514/1.A34821>.
- [45] Grigat, F., Löhle, S., Zander, F., and Fasoulas, S., “Spallation on Carbon Ablators,” *AIAA Journal*, Vol. 60, No. 7, 2022, pp. 3936–3949. <https://doi.org/10.2514/1.J061276>.
- [46] Buquet, M., Glenn, A., Collen, P., Williams, B., McGilvray, M., and Hermann, T., “Design of a Spatially Resolved VUV Spectroscopy System for Shock Tube Flows,” *9th International Workshop on Radiation of High Temperature Gases for Space Missions*, 2022.
- [47] Sakraker, I., Chazot, O., and Carvalho, J. P., “Performance of cork-based thermal protection material P50 exposed to air plasma,” *CEAS Space Journal*, Vol. 14, 2022, pp. 377–393. <https://doi.org/10.1007/s12567-021-00395-z>.
- [48] Hyslop, A., Doherty, L. J., McGilvray, M., Neely, A., McQuellin, L. P., Barth, J., and Mullen, G., “Free-Flight Aerodynamic Testing of the Skylon Space Plane,” *Journal of Spacecraft and Rockets*, Vol. 58, No. 5, 2021, pp. 1487–1497. <https://doi.org/10.2514/1.A34937>.
- [49] COMSOL Multiphysics, “Introduction to COMSOL multiphysics®,” 1998, p. 2018.
- [50] Dassault Systèmes, “SolidWorks®,” 2018.